Endosidin 7 Specifically Arrests Late Cytokinesis and Inhibits Callose Biosynthesis, Revealing Distinct Trafficking Events during Cell Plate Maturation[1][W][OPEN]

Eunsook Park, Sara M. Díaz-Moreno, Destiny J. Davis, Thomas E. Wilkop, Vincent Bulone, and Georgia Drakakaki*

Department of Plant Sciences, University of California, Davis, California 95616 (E.P., D.J.D., T.E.W., G.D.); and Division of Glycoscience, School of Biotechnology, Royal Institute of Technology, AlbaNova University Centre, 106 91 Stockholm, Sweden (S.M.D.-M., V.B.)

ORCID ID: 0000-0003-2984-3039 (E.P.).

Although cytokinesis is vital for plant growth and development, our mechanistic understanding of the highly regulated membrane and cargo transport mechanisms in relation to polysaccharide deposition during this process is limited. Here, we present an in-depth characterization of the small molecule endosidin 7 (ES7) inhibiting callose synthase activity and arresting late cytokinesis both in vitro and in vivo in Arabidopsis (*Arabidopsis thaliana*). ES7 is a specific inhibitor for plant callose deposition during cytokinesis that does not affect endomembrane trafficking during interphase or cytoskeletal organization. The specificity of ES7 was demonstrated (1) by comparing its action with that of known inhibitors such as caffeine, flufenacet, and concanamycin A and (2) across kingdoms with a comparison in yeast. The interplay between cell plate-specific post-Golgi vesicle traffic and callose accumulation was analyzed using ES7, and it revealed unique and temporal contributions of secretory and endosomal vesicles in cell plate maturation. While RABA2A-labeled vesicles, which accumulate at the early stage of cell plate formation, were not affected by ES7, KNOLLE was differentially altered by the small molecule. In addition, the presence of clathrin-coated vesicles in cells containing elevated levels of callose and their reduction under ES7 treatment further support the role of endocytic membrane remodeling in the maturing cell plate while the plate is stabilized by callose. Taken together, these data show the essential role of callose during the late stages of cell plate maturation and establish the temporal relationship between vesicles and regulatory proteins at the cell plate assembly matrix during polysaccharide deposition.

During plant cytokinesis, the de novo formation of a new cell wall partitions the cytoplasm of the dividing cell (Staehelin and Hepler, 1996; Jürgens, 2005). The formation of the transient cell plate structure is a complex multistep process (Samuels et al., 1995; Jürgens, 2005). At the end of late anaphase, vesicle delivery is guided by the phragmoplast to the center of the dividing cell, the cell plate assembly matrix (CPAM; Samuels et al., 1995). Vesicles at the CPAM undergo homotypic fusion and fission, contributing to the formation of the incipient cell plate (Jürgens, 2005). The initial vesicular fusion and fission events (fusion of Golgi-derived vesicles stage [FVS]) lead to the formation of a tubulovesicular network (TVN), which undergoes a morphological change to form a tubular network (TN). Callose deposition starts during this stage (Supplemental Fig. S1), which is thought to provide mechanical support to the membrane network that ultimately results in the planar fenestrated sheet (PFS). The cell plate expands centrifugally by the accumulation and fusion of newly arriving vesicles at its leading edge. This process is accompanied by the accumulation of new polysaccharides and the removal of excess material maturing at the center. Separation of the daughter cells concludes by fusion of the cell plate with the parental plasma membrane (Samuels et al., 1995).

A vast amount of proteins including those involved in vesicle trafficking participate in cell plate formation (McMichael and Bednarek, 2013). Vesicle fusion with the target membrane is mediated by the formation of Soluble *N*-ethylmaleimide-sensitive factor protein attachment protein receptor (SNARE) complexes (Bassham and Blatt, 2008). The well-characterized SNARE complex at the cell plate comprises the Q-SNARE KNOLLE and the functionally redundant R-SNARES, the vesicle-associated membrane proteins VAMP721 and VAMP722 (Lauber et al., 1997; Zhang et al., 2011; El Kasmi et al., 2013). The SEC1/Munc18 protein KEULLE, the Soluble N-ethylmaleimide-sensitive factor adaptor protein33, and the novel plant-specific SNARE11 (Assaad et al., 2001; Heese et al., 2001; Zheng et al., 2002) play a role in this SNARE

[1] This work was supported by the National Science Foundation (grant no. IOS–1258135 to G.D.), by University of California, Davis (startup funds to G.D.), and by the Royal Institute of Technology Advanced Carbohydrate Materials Consortium (grant to V.B. from the Swedish Research Council for Environment, Agricultural Sciences, and Spatial Planning).

* Address correspondence to gdrakakaki@ucdavis.edu.

The author responsible for distribution of materials integral to the findings presented in this article in accordance with the policy described in the Instructions for Authors (www.plantphysiol.org) is: Georgia Drakakaki (gdrakakaki@ucdavis.edu).

[W] The online version of this article contains Web-only data.

[OPEN] Articles can be viewed online without a subscription.

www.plantphysiol.org/cgi/doi/10.1104/pp.114.241497

complex formation. Of all the SNAREs required for vesicle fusion at the cell plate, only KNOLLE has been shown to function exclusively in cytokinesis.

The formation of the cell plate requires specific amounts of vesicle-delivered membrane and other secretory products. The GTPase RABA2A is necessary for the delivery of trans-Golgi network (TGN)-derived vesicles to the cell plate leading edge (Chow et al., 2008). However, due to the excess delivery of material arriving at the cell plate formation site, it is estimated that 70% is recycled (Samuels et al., 1995; Otegui et al., 2001). Electron microscopy observations indicate the role of clathrin-coated vesicles (CCVs) in the removal and/or recycling of excess membranes from the cell plate (Samuels et al., 1995; Otegui and Staehelin, 2004; Seguí-Simarro et al., 2004). Specifically, clathrin light chain (CLC), dynamin-related proteins (DRPs), the adaptin-like TPLATE, and AP180 amino-terminal homology/epsin amino-terminal homology domain-containing protein have been identified at the cell plate, providing evidence that clathrin-mediated endocytosis facilitates this membrane recycling (Konopka et al., 2008; Konopka and Bednarek, 2008; Fujimoto et al., 2010; Van Damme et al., 2011; Ito et al., 2012; Song et al., 2012; McMichael and Bednarek, 2013). In addition, it has been suggested that plasma membrane endocytosis contributes material toward de novo cell plate formation (Dhonukshe et al., 2006). However, the level of endocytosis involvement remains questionable, as pharmacological inhibition of endocytosis does not interfere with cytokinesis (Reichardt et al., 2007). The temporal association of different vesicle populations at the CPAM might provide further insights into their contribution to the forming cell plate.

Despite the large number of studies investigating membrane dynamics, relatively few studies exist on polysaccharide deposition during cell plate maturation. It has been suggested that callose, a (1,3)-β-glucan, stabilizes the delicate tubular network during the initial cell plate formation stage, until the deposition of additional polysaccharides increases its rigidity (Samuels et al., 1995). Callose accumulation is transient, with the polymer being removed once other polysaccharides such as hemicelluloses, pectins, and cellulose are deposited at the cell plate (Supplemental Fig. S1; Samuels et al., 1995; Albersheim et al., 2010). The timing of callose deposition at the cell plate in relation to that of vesicle trafficking that contributes to cell plate formation is unknown.

Genetic studies have indicated a role of callose accumulation at the cell plate (Chen et al., 2009; Thiele et al., 2009; Guseman et al., 2010). However, the lethality of mutant alleles for the callose synthase/glucan synthase-like family (GSL) has hampered the detailed examination of the role of callose synthase and its product in cell plate maturation (Verma and Hong, 2001; Chen et al., 2009; Thiele et al., 2009; Guseman et al., 2010). The ability to transiently perturb callose deposition at the cell plate is key to understanding callose's contribution to the separation of the daughter cells compared with other polysaccharides.

Here, we used pharmacological inhibitors to overcome the challenges of the lethality of callose synthase mutants. In a high-throughput confocal microscopy-based screen for small molecules affecting endosomal trafficking (Drakakaki et al., 2011), endosidin 7 (ES7) was identified as an inhibitor of cell plate formation. ES7 induces characteristic cell plate gaps, observable by the mislocalization of KNOLLE and RABA2A, while it does not affect the localization of endomembrane compartment markers in interphase cells. The potential of ES7 to inhibit callose deposition at the cell plate (Drakakaki et al., 2011) provides avenues to study cell plate maturation. We have characterized the activity of ES7 using both in vitro and in vivo studies establishing its inhibitory effects on callose biosynthesis. We have exploited the properties of ES7 to characterize in detail callose deposition at the cell plate, thereby providing further insight into the overall cell plate formation process. Our results conclusively show that callose is essential for the later stages of cell plate maturation and lay out the temporal association and interplay of TGN and endosomal vesicles during polysaccharide deposition.

RESULTS

ES7 Interrupts Cytokinesis and Inhibits Plant Growth

The cell plate formation and growth of Arabidopsis (*Arabidopsis thaliana*) seedlings were examined in the presence of ES7 to gain insight into the effect of the drug on plant development. A 2-h pulse treatment with 50 μM ES7 induced characteristic cell plate gaps and fragmented cell plates, as observed with FM4-64 staining and the aid of the cell plate-localized yellow fluorescent protein (YFP)-RABA2A at the root tip division zone (Fig. 1, A and B). In three-dimensional micrograph reconstructions, cell plate stubs are visible and disconnected from the parental cell wall (magenta arrow in Supplemental Fig. S2B). This incomplete cytokinesis leads to the formation of binucleate cells (Fig. 1C), a common feature of mutants exhibiting impaired cell division, even at 25 μM ES7. In contrast, the dimethyl sulfoxide (DMSO) control treatment has no effects on the cell plate during each cytokinetic stage (Fig. 1A; Supplemental Fig. S2A).

The bioactivity of ES7 in seedlings was further assessed by examining cell division patterns and quantifying growth. ES7 strongly altered the cell file pattern in root tips. Cellular organization became more irregular with concurrent loss of symmetry (Fig. 2, A and B), both of which are phenotypic hallmarks of cytokinesis-defective mutants (Söllner et al., 2002). These defects are not restricted to root cells but also extend to the cotyledons. Incomplete cell walls in cotyledons are clearly observable in the ES7-treated samples (Fig. 2, C and D). Furthermore, seedling growth was reduced by ES7 in a concentration-dependent manner (Fig. 2E). Seedling growth is

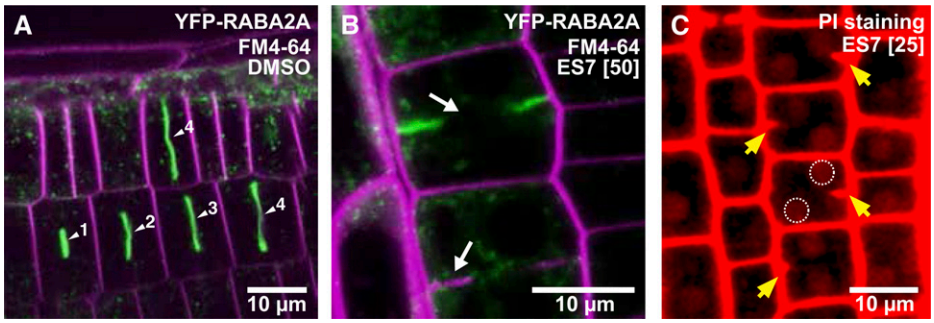

Figure 1. Inhibition of cell plate maturation by ES7 in Arabidopsis root cells. A, DMSO control treatment. From the early cell plate formation steps, YFP-RABA2A-labeled vesicles strongly accumulate at the cell plate. Numbers next to arrowheads indicate the relative stage of cell plate maturation. Counterstaining of the plasma membrane with FM4-64 is indicated in magenta, while YFP-RABA2A is presented in green. B, Pulse treatment with 50 μM ES7 for 2 h causes characteristic cell plate gaps observed by FM4-64 staining and mislocalization of YFP-RABA2A (white arrows). C, PI staining of the ES7-treated root shows binucleated cells, highlighted by perforated circles. Cell wall stubs indicating that double nuclei are caused by incomplete cell division are marked by yellow arrows.

arrested and leads to lethality at 25 μM, which suggests that this dose is sufficient to strongly inhibit cell division. The half-maximal inhibitory concentration of ES7 is 4.8 μM as determined by root growth assays (Fig. 2F). These data show that ES7 hinders somatic cytokinesis and is a potent inhibitor of plant growth. Five and 10 μM concentrations of ES7 were selected for root growth assays. These concentrations result in 50% and 80% inhibition of root growth, respectively. Higher concentrations (25 and 50 μM) were used for 2-h pulse treatments of subcellular effects (Drakakaki et al., 2011).

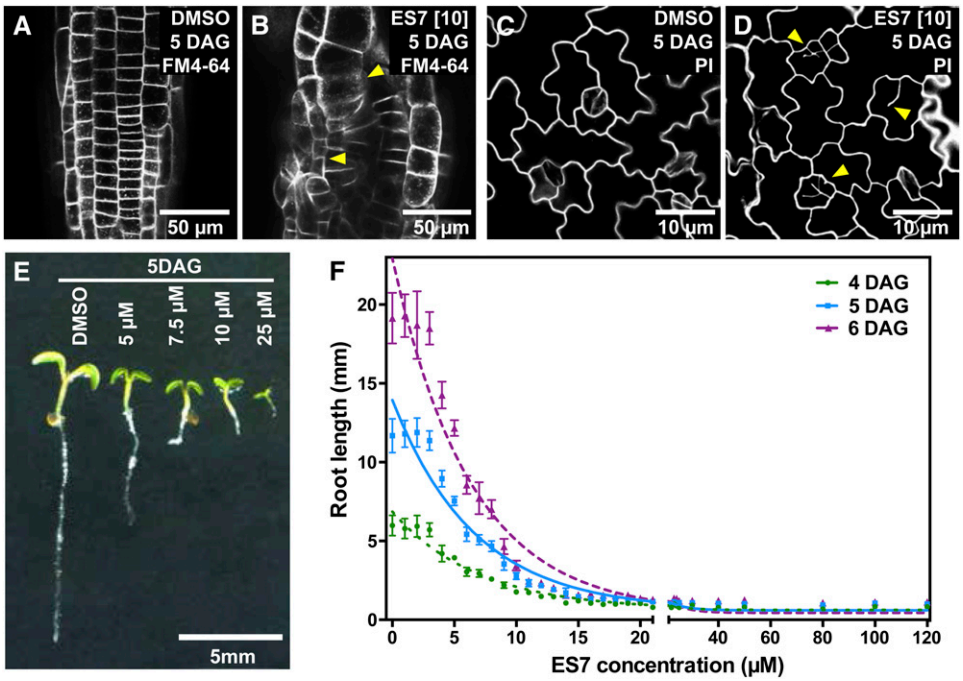

Figure 2. ES7 treatment results in concentration-dependent growth inhibition of Arabidopsis seedlings. A and B, Arabidopsis roots at 5 d after germination (DAG) stained by FM4-64. While roots grown with DMSO display regular cell organization (A), exposure to ES7 causes the collapse of root tissue organization and abnormal cell sizes (yellow arrowheads in B). C and D, PI staining of leaf pavement cells. Seedlings grown under 10 μM ES7 for 5 d show cell wall stubs and result in fewer guard cells at the epidermis (yellow arrowheads in D) compared with cotyledons grown under DMSO (C). E, ES7 dosage-dependent inhibition of 5-d-old seedling root growth. F, Dosage-dependent root growth of Arabidopsis seedlings over an ES7 concentration gradient. The half-maximal inhibitory concentration is calculated to be 4.8 μM for root growth of 5-d-old seedlings, with $n > 48$. Seedlings were imaged and root lengths were measured at 4 DAG (green circles), 5 DAG (blue squares), and 6 DAG (purple triangles). Trend lines were generated by a one-phase exponential decay curve fit ($r^2 > 0.9$).

ES7 Is a Plant-Specific Cytokinesis Inhibitor

The inhibition of callose at the cell plate was investigated by immunostaining. A concentration-dependent inhibition of callose deposition was observed in ES7-treated plants (Fig. 3), which demonstrates the activity of ES7 on this polysaccharide. Interestingly, while callose deposition was not detectable upon 25 μM ES7 treatment (Fig. 3D), cells treated with lower concentrations displayed visible, albeit abnormal, deposition of callose at the cell plate (Fig. 3, B and C).

Callose deposition at the cell wall occurs in a number of different biological events (Verma and Hong, 2001). We investigated whether ES7 is a plant-specific inhibitor and if it affects callose deposition only during cytokinesis and not in other developmental processes in which callose plays a role (Supplemental Fig. S3). Callose accumulation in physically wounded plants was not affected by ES7 (Supplemental Fig. S3, B and E). However, its effect on cytokinesis in the same tissues was apparent (Supplemental Fig. S3, C and F); this indicates that the inhibition of cytokinesis does not influence stress-induced callose deposition.

Similarly ES7 did not affect callose plug formation in sieve elements (Supplemental Fig. S3, G and H). This observation was not due to limited uptake, because cell plate defects in the neighboring cells of sieve elements were apparent in the same root tissues. Altogether, these data support the specificity of ES7 on cytokinesis-associated callose deposition. As noted previously (Drakakaki et al., 2011), ES7 treatment suppressed pollen germination (Supplemental Fig. S3J).

(1,3)-β-Glucans similar to callose are major structural components of yeast (*Saccharomyces cerevisiae*) cell walls, and the corresponding *S. cerevisiae* (1,3)-β-glucan synthase shares structural similarities with Arabidopsis GSLs (Hong et al., 2001). In order to test the specificity of ES7 on plant callose synthases, we evaluated yeast cell growth over a range of ES7 concentrations, including those that are lethal for plants (Supplemental Fig. S4). ES7 treatment did not measurably affect yeast population growth over periods of 24 and 48 h (Supplemental Fig. S4), which underscores its specific activity on plants.

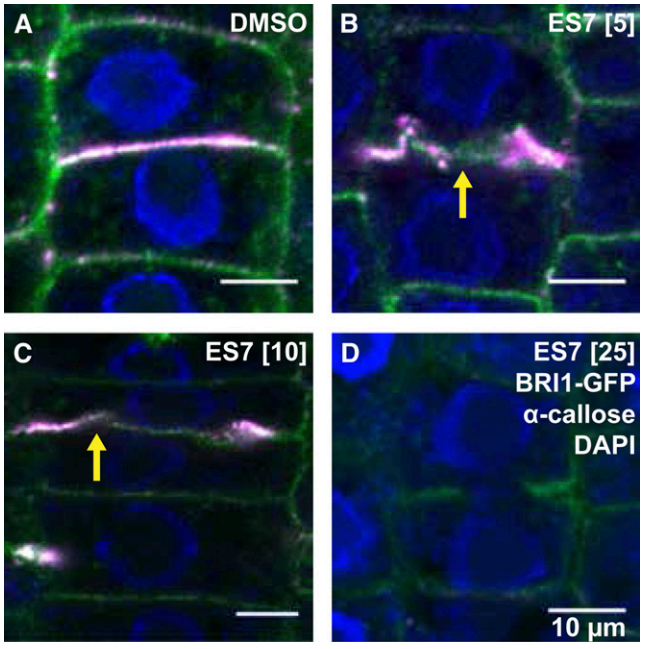

Figure 3. Concentration-dependent inhibition of callose accumulation at the cell plate. A, Control cells were treated with DMSO. B, A 5 μM ES7 treatment caused abnormal accumulation of callose at the cell plate. C, A 10 μM ES7 treatment displayed less callose deposition at the cell plate than DMSO or 5 μM ES7 treatment. Note that BRI1-GFP accumulation at the center of the cell plate formation site is still visible (yellow arrows in B and C). D, Callose deposition at the cell plate disappears under 25 μM ES7 treatment. Plasma membrane labeling of BRI1-GFP is shown in green, α-callose in red, and DAPI nuclear staining in blue. All treatments were 2 h long. Bars = 10 μm.

ES7 Inhibits Callose Synthase Activity

The effect of ES7 on callose synthase activity was investigated by employing a well-established assay using CHAPS extracts of Arabidopsis cell membranes as an enzyme source. Previous studies using permethylation linkage analysis, ^{13}C-NMR spectroscopy, and x-ray diffraction unequivocally showed that callose is the only polysaccharide synthesized under these in vitro conditions (Him et al., 2001). Assays of callose synthase activity in the presence of 0 to 100 μM ES7 revealed a concentration-dependent decrease (Fig. 4A). One hundred micromolar ES7 reduced the activity of the enzyme by 50%. In order to understand the mode of action of ES7, enzyme kinetics were determined in the presence of 0, 40, and 80 μM ES7 (Fig. 4B). The data revealed that increasing concentrations of ES7 were accompanied by higher apparent K_m and lower V_{max} values compared with the control. For the two concentrations of ES7 tested, the apparent association constant of ES7 to the enzyme-substrate complex measured in the presence of the inhibitor was twice as high as the apparent association constant of ES7 to the free enzyme, indicating that ES7 acts as a mixed-type inhibitor that may interact directly or indirectly with the free enzyme and with the enzyme-substrate (UDP-Glc) complex with a different affinity.

Cellulose Deposition Is Not Inhibited by ES7

Cellulose, a (1,4)-β-glucan, accumulates at later stages of cell plate formation (Samuels et al., 1995). To further examine the specificity of ES7 on both Glc-based polysaccharides (cellulose and callose), we examined cellulose localization after chemical treatment. There was no discernible difference in Glc labeling between DMSO- and ES7-treated sections (Supplemental Fig. S5, A and B). Average fluorescence intensity values for labeled cellulose in tissues incubated in the presence and absence of ES7 did not differ by more than 4%. In addition, root

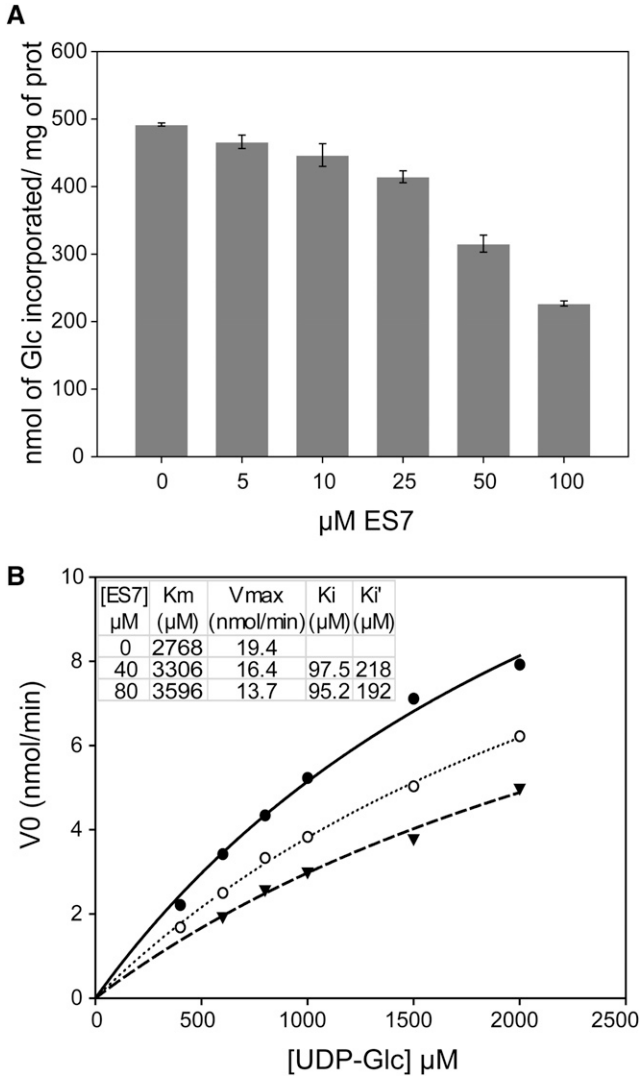

Figure 4. Concentration-dependent inhibition of callose synthase activity by ES7. A, Callose synthase activity in Arabidopsis microsome extracts, measured in the presence of 1 mM UDP-Glc over a range of ES7 concentrations. B, Michaelis-Menten kinetics of callose synthase activity in the absence of ES7 (solid line) and in the presence of 40 μM (dotted line) and 80 μM (dashed line) ES7. Initial velocities V0 (nmol/min) for different chemical concentrations are shown. The apparent K_m, V_{max}, and association constants of ES7 to the free enzyme (K_i) and to the enzyme-substrate complex (K_i') for the three cases are shown.

growth of *procuste1*, a mutant allele for the CELLULOSE SYNTHASE6 (CESA6) subunit (Fagard et al., 2000), was strongly inhibited by ES7 treatment (Supplemental Fig. S5C), providing further evidence of the specificity of ES7 toward callose deposition.

ES7 Inhibits the Late Steps of Cell Plate Formation

As stated above, cell plate formation follows distinct developmental stages (Samuels et al., 1995; Supplemental Fig. S1). We refer to the stage in which Golgi-derived vesicles are fusing as an early stage, while the formation of TVN, TN, and PFS is referred to as later stages. To dissect vesicle dynamics in cell plate formation, we investigated the effects of ES7 on the localization of the fluorescent cell plate markers (Supplemental Table S1) YFP-RABA2A (Chow et al., 2008), KNOLLE-GFP (Reichardt et al., 2007), DRP1C-GFP and CLC2-GFP (Kang et al., 2003; Konopka et al., 2008) at early and later stages. These proteins were selected for their known roles in cell plate formation.

In the meristematic zone of Arabidopsis root tips treated with DMSO, YFP-RABA2A was found to accumulate at the cell plate in two distinct forms: (1) as a disc-like pattern during the early stages and (2) as a ring-type pattern in later stages (Fig. 5, A and G; Supplemental Fig. S2A). This developmental pattern agrees well with previous observations in Arabidopsis root tips (Chow et al., 2008). Since the cell plate matures centrifugally, a disc-like cell plate structure contains several stages of maturation, with the early stage being located on the circumference of the plate (Supplemental Fig. S1). While both disc- and ring-type structures of YFP-RABA2A accumulation at the cell plate were unaffected by DMSO (Fig. 5, A and G; Supplemental Fig. S2A, white and yellow arrows), ES7 affected the two accumulation patterns in a different manner. While disc-like accumulations were not affected (Fig. 5D; Supplemental Fig. S2B, white arrow), ring-shaped YFP-RABA2A structures exhibited characteristic gaps (Fig. 5K; Supplemental Fig. S2B, yellow arrow). This differential behavior indicates that ES7 inhibits the later stages of cell plate maturation.

Additional marker proteins involved in cell plate formation were analyzed to further corroborate the observed late-stage effects of ES7 (Fig. 5). KNOLLE is exclusively expressed in dividing cells throughout cytokinesis (Lauber et al., 1997). In the presence of ES7, KNOLLE-GFP showed normal accumulation at the center of the dividing cells during the early stages of cell plate formation (Fig. 5, E and B). This contrasted with the behavior of KNOLLE-GFP during the late stages of cell plate formation, in which the protein accumulated in stubs exhibiting a massive lateral expansion (Fig. 5, L and H). DRPs are present in early and late stages of cell plate formation (Otegui et al., 2001; Collings et al., 2008; Konopka et al., 2008). It has been postulated that, together with CLC, DRPs are involved in endocytosis at late stages, thereby promoting cell plate maturation (Konopka et al., 2008; Fujimoto et al., 2010). While DRP1C-GFP proteins were identifiable at an early cell plate stage (Fig. 5, C and F), CLC2-GFP accumulations were not detectable at the same stage. However, both proteins accumulated in mature cell plates (Fig. 5, I and J). In the presence of ES7, DRP1C-GFP displayed abnormal accumulation only in mature cell plates (Fig. 5M), while CLC2-GFP patterns remained punctate, with preferred localizations at the cell plate stub (Fig. 5N).

Taken together, these data conclusively demonstrate that ES7 exerts its inhibitory effects only during the later

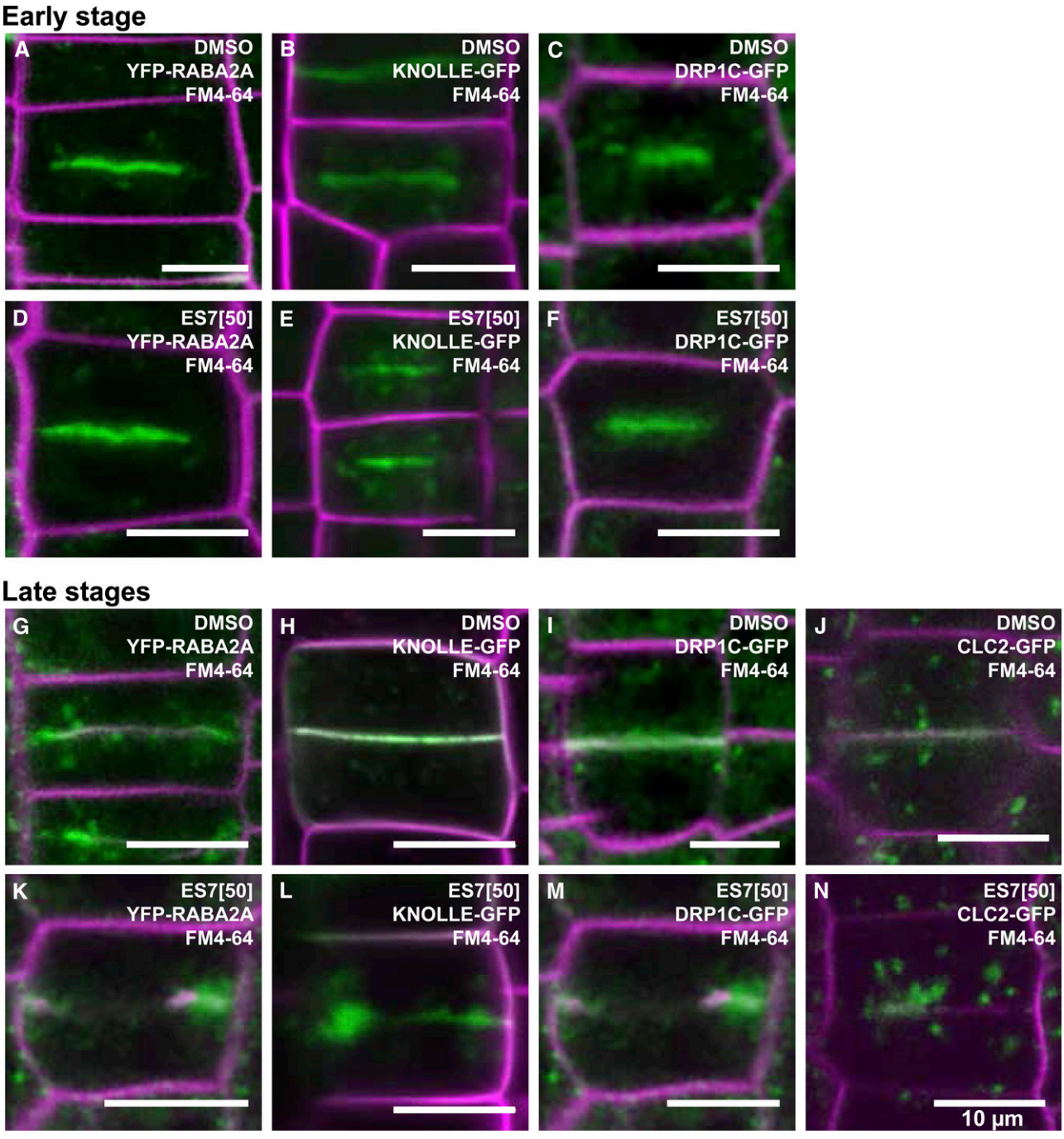

Figure 5. ES7 inhibits later stages of cell plate maturation. In the early steps of cell plate formation, YFP-RABA2A (A), KNOLLE-GFP (B), and DRP1C-GFP (C) accumulate at the center of the dividing cell. Early-stage cell plates labeled by these markers are not affected by ES7 (D–F). During later stages of cell plate maturation, YFP-RABA2A largely accumulates at the edge of the growing cell plate (G), KNOLLE-GFP and DRP1C-GFP localize along the cell plate (H and I), and CLC2-GFP shows relatively low levels of cell plate accumulation while localizing in the vicinity of the cell plate (J). During later maturation stages, ES7 causes split cell plates with abnormal accumulation of the markers (K–N). Note the aggregation of KNOLLE-GFP at cell plate stubs (L). FM4-64 counterstaining of the plasma membrane is indicated by magenta, and the respective markers are indicated in green. Bars = 10 μm.

steps of cell plate maturation and that vesicle accumulation at the plane of division during the early stage of cell plate formation is unaffected. Furthermore, these results show that ES7 exerts its inhibitory effect differentially for specific vesicle populations, which depends on both their function and the timing of accumulation at the CPAM.

Interplay of Vesicle Accumulation and Callose Deposition during Cell Plate Maturation

To further understand the timely contribution of vesicle populations to cell plate maturation, we followed protein localization in relation to callose deposition at the cell plate (Fig. 6). In early cell plate formation steps, YFP-RABA2A, KNOLLE-GFP, or DRP1C-GFP strongly accumulated at the center of the dividing cells, whereas callose did not accumulate (Fig. 6, A, D, and G, respectively). During later stages, YFP-RABA2A localized at the leading edge of the growing cell plate (Fig. 6B; Supplemental Movie S1), whereas KNOLLE-GFP (Fig. 6E; Supplemental Movie S2) and DRP1C-GFP accumulation was uniform along the cell plate (Fig. 6H). Callose deposition was initially observed at this stage (Fig. 6, B, E, and H, yellow arrowheads). Interestingly, callose deposition at the cell plate was accompanied by a reduction in YFP-RABA2A accumulation (Fig. 6C), while the accumulation of the KNOLLE-GFP protein was unaltered (Fig. 6F). Although DRP1C-GFP exhibited even accumulation along the cell plate, similar to KNOLLE-GFP, its level of accumulation was reduced at stages where callose deposition started, compared with early cell plate stages (Fig. 6, G–I). CLC2-GFP was not observed at early stages, but its occurrence was occasionally detectable in expanding cell plates (Fig. 6J). However, concurrent with callose deposition, CLC2-GFP enrichment at the cell plate was observed (Fig. 6, K and L).

No callose deposition is detectable at the cell plate upon ES7 treatment (Fig. 7). The absence of callose at the early stages of cell plate development (Fig. 7, A, C, and E) did not cause any cell plate defects. At later stages of cell plate formation, the absence of callose is accompanied by characteristic cell plate defects, which are identified by the markers YFP-RABA2A, KNOLLE-GFP, and DRPC1C-GFP (Fig. 7, B, D, and F; Supplemental Movies S3 and S4). Interestingly, KNOLLE-GFP displayed abnormal highly voluminous aggregates at the cell plate stubs (Fig. 7D), implying that the lack of callose at the cell plate arrests the expansion of the existing TVN/TN, leading to aggregations of the syntaxin KNOLLE. The CLC2-GFP pattern remained punctate under ES7 treatment (Fig. 7G).

These results establish the timing of ES7 concurrent with callose deposition. In addition, they show the role of callose in TVN/TN maturation and the association of the polysaccharide with a specific vesicle population at the CPAM.

ES7 Is a Highly Specific Inhibitor for Callose Deposition at the Cell Plate Compared with Known Cytokinesis Inhibitors

Several small molecules acting as inhibitors of endomembrane trafficking have been used to perturb cell plate formation. For example, concanamycin A (ConcA), a vacuolar type H^+-ATPase inhibitor (Dröse et al., 1993; Huss et al., 2002), blocks TGN-mediated vesicle trafficking (Dettmer et al., 2006). Flufenacet inhibits the synthesis of long-chain fatty acids (Bach et al., 2011). Caffeine affects cytoskeletal organization and callose deposition, resulting in fragmented cell plates (Jones and Payne, 1978; Samuels and Staehelin, 1996; Yasuhara, 2005). We compared the response of ES7 with that of the above-mentioned inhibitors and investigated their activities on a variety of marker protein localizations and callose deposition at the cell plate. The selected markers were YFP-RABA2A as an early cell plate marker, GFP-microtubule-associated protein4 (GFP-MAP4) as a microtubule marker, and the cellulose synthase GFP-CESA3 as a marker for Golgi- and microtubule-associated vesicles (Supplemental Table S1).

In living cells, ES7, caffeine, flufenacet, and ConcA treatments resulted in characteristic split cell plate formation, as shown by YFP-RABA2A (Fig. 8, B–E). Phragmoplast formation was normal upon ES7 and ConcA treatments (Fig. 8, G and J). However, flufenacet treatment led to ectopic phragmoplast formation at the mature cell plate (Fig. 8I). Caffeine changed the morphology of the phragmoplast in a way that is somewhat similar to that of a mitotic spindle (Fig. 8H). In addition, microtubule aggregation in the interphase cells was induced by caffeine (Supplemental Fig. S6G, white arrow). Recent studies showed that cellulose synthase proteins localize at the cell plate during cytokinesis (Miart et al., 2014). A partial vacuolar-type organization was observed for GFP-CESA3 dividing cells treated with ES7, while a normal localization was observed in interphase cells (Fig. 8L; Supplemental Fig. S6B). Interestingly, GFP-CESA3 aggregated upon caffeine treatment, with many of these aggregates localizing adjacent to the cell wall (Fig. 8M, white arrow), probably due to abnormal microtubule organization (Fig. 8H; Supplemental Fig. S6G). Furthermore, the ring-type fluorescence of GFP-CESA3 was observed in interphase cells (Supplemental Fig. S6C). Flufenacet treatment caused severe aggregation of the CESA3 complexes in both dividing and interphase cells (Fig. 8N; Supplemental Fig. S6D), while ConcA led to their vacuolization (Fig. 8O). ES7 and caffeine caused inhibition of callose at the cell plate (Fig. 8, Q and R), while flufenacet did not (Fig. 8S). Taken together, these data demonstrate that ES7 does have a distinct mode of action that differs markedly from that of the other cytokinesis inhibitors.

DISCUSSION

In this report, we characterized the distinct effects of ES7 on cell plate formation and the inhibition of callose synthase activity and investigated the interplay of secretory vesicle trafficking with callose deposition at the cell plate.

ES7 Affects a Cytokinesis-Specific Callose Deposition Pathway

Although the involvement of callose in cell plate maturation has been documented, detailed genetic

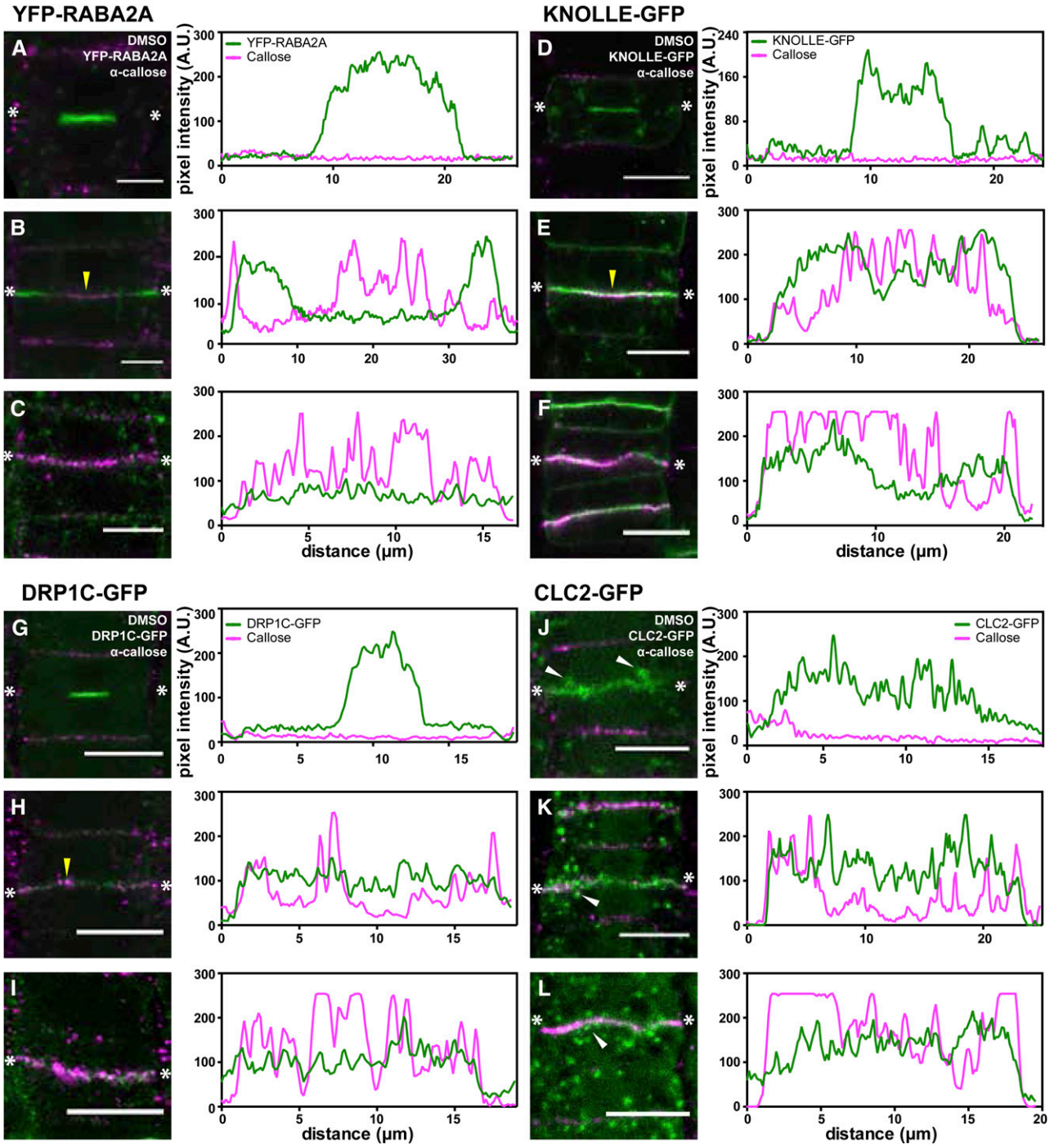

Figure 6. Differential vesicle accumulation occurs during callose deposition at the cell plate. Immunostaining of callose is shown with respect to the localization of vesicle markers involved in cell plate formation. Representative cells at different cell plate maturation stages are shown, and fluorescence intensities are plotted in line profiles, as indicated with the two asterisks, reflecting the fluorescence at the center of the cell plate. Throughout, α-callose is marked in magenta, while the respective fluorescent markers are indicated in green. A to C, YFP-RABA2A-labeled vesicles largely accumulate at the center of the cell during early stages, in which callose is not detectable (A). In later stages (B), YFP-RABA2A is localized at the leading edge of the cell plate, while callose started accumulating (yellow arrowhead). With the callose accumulation increasing along the cell plate, the presence of YFP-RABA2A is reduced concomitantly (C). D to F, Similar to YFP-RABA2A, KNOLLE-GFP accumulates at the center of the cell during the FVS (D). However, unlike for YFP-RABA2A, the accumulation of KNOLLE-GFP remains the same during callose deposition (E and F). G to I, The DRP1C-GFP accumulation pattern is similar to that of KNOLLE-GFP. Vesicles accumulate along the cell plate in the FVS (G) and throughout the later stages when callose strongly accumulates (H and I). J to L, No cells labeled with CLC2-GFP undergoing the FVS are observable. Occasionally, CLC2-GFP is

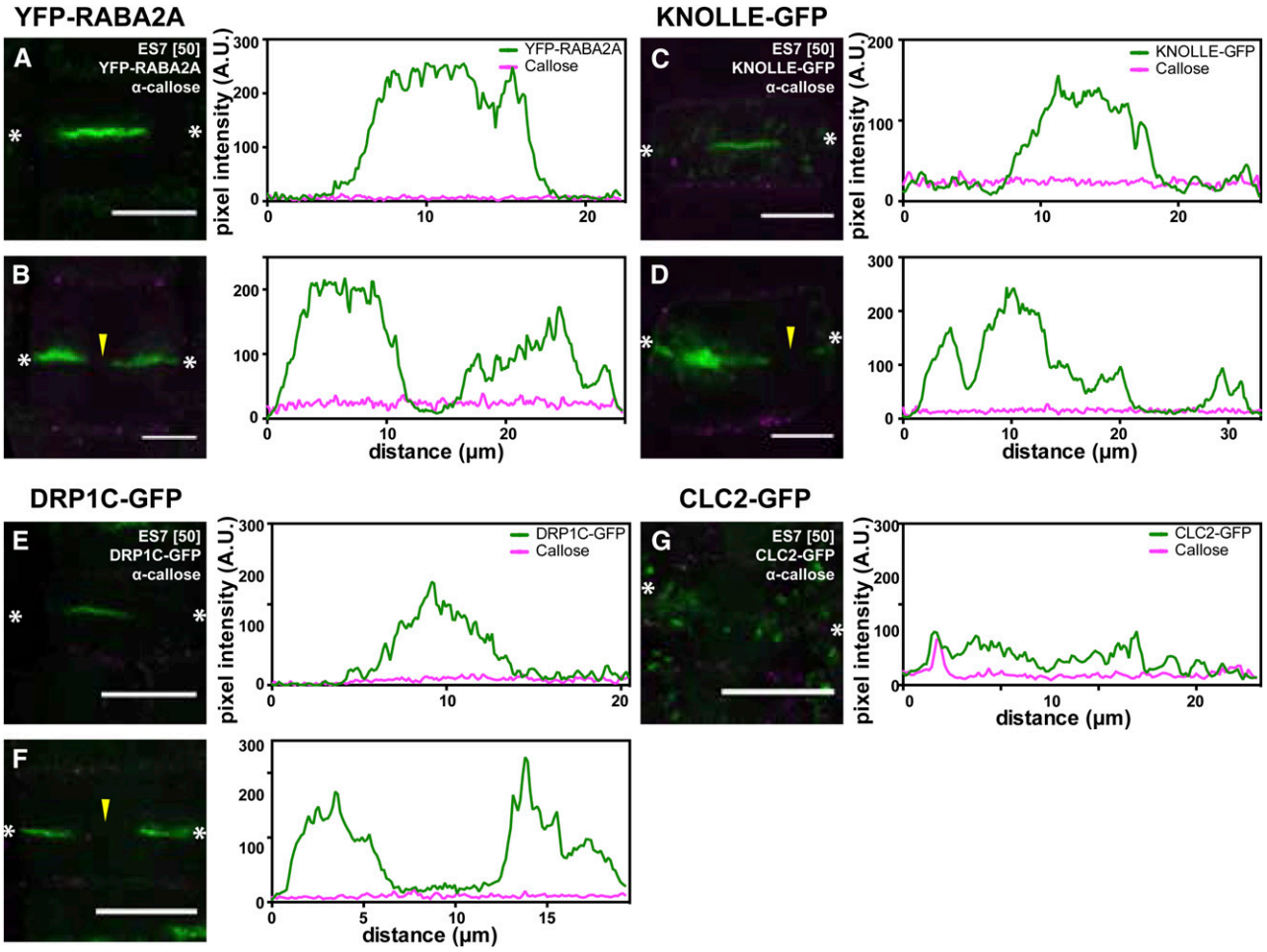

Figure 7. ES7 inhibits cell plate maturation after FVS. A, C, and E, Vesicle accumulation during the FVS is not affected by ES7. B, D, F, and G, A 2-h treatment with 50 μM ES7 abolished callose deposition at the cell plate, arresting cell plate maturation. This is indicated by the absence of the fluorescent markers in the center of the plate (arrowheads), normally the site of callose deposition. Note the aggregation of KNOLLE (D). No cell plate localization of CLC2-GFP is detectable (G). α-Callose is marked in magenta, while the respective fluorescent markers are indicated in green. A.U., Arbitrary units. Bars = 10 μm.

studies are challenging due to the lethality typically associated with cytokinesis alterations (Samuels et al., 1995; Thiele et al., 2009; Worden et al., 2012). To overcome this, temporal inhibition with a chemical inhibitor approach can be employed. Here, we describe the specific inhibition of callose deposition during cytokinesis by the small molecule ES7. Biochemical assays are consistent with the microscopic observations at the cell plate and demonstrate the inhibitory effect of ES7 on callose biosynthesis in vitro and in vivo. Cellulose and callose are both synthesized from UDP-Glc, and both are present at the cell plate (Samuels et al., 1995; Miart et al., 2014). However, cellulose deposition was shown to be insensitive to the ES7 treatment, thereby indicating a high specificity of the drug for callose biosynthesis. Callose accumulation plays a role in several aspects of plant development and is not restricted to cytokinesis. The polysaccharide can be found in abundance in plasmodesmata, sieve plates, pollen mother cells, pollen tubes, and root hairs. Callose accumulation can also be induced by pathogens, wounding, and environmental stresses (Chen and Kim, 2009). ES7 does not inhibit callose accumulation at the sieve element or in response to wounding, while it exerts its inhibitory effects on cytokinesis in the same tissues. This demonstrates that the specificity

Figure 6. (*Continued.*)
observed in expanded cell plates without callose deposition, possibly representing an early TVN stage (J). Accumulation of CLC2-GFP at the cell plate does not change between the later stages of cell plate maturation (K and L). Note the increased vesicle localization in the proximity of the cell plate (white arrowheads in J–L). A.U., Arbitrary units. Bars = 10 μm.

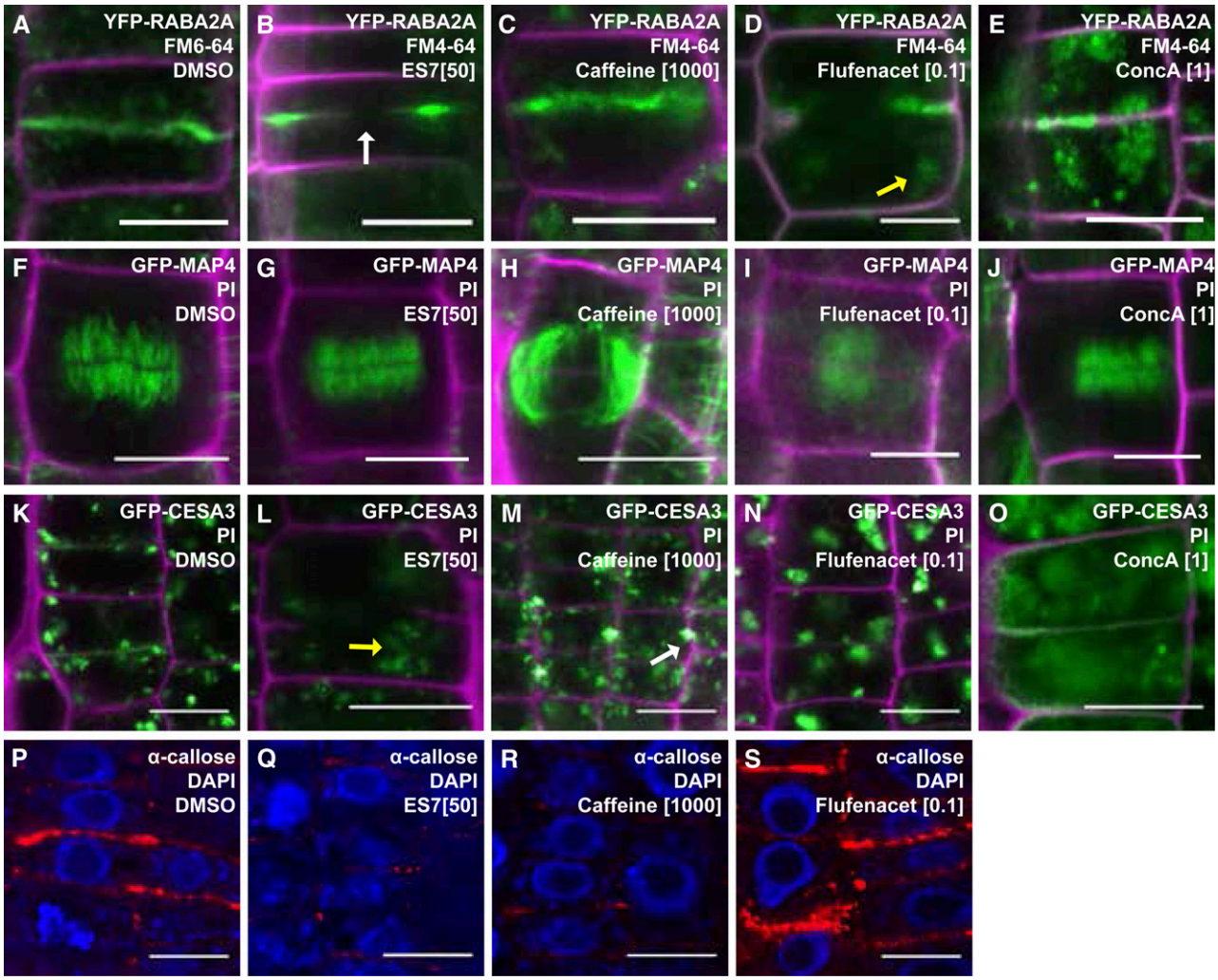

Figure 8. ES7 specifically affects callose deposition at the cell plate and no other cellular components. The effect of ES7 and other known cytokinesis inhibitors on the localization of subcellular markers and callose deposition is compared. A to E, YFP-RABA2A-labeled cells after drug treatments. Under DMSO treatment, YFP-RABA2A accumulates at the leading edge of the expanding cell plate at a 100% frequency (A). Under ES7 treatment, YFP-RABA2A and FM4-64 accumulation shows characteristic cell plate gaps at an 87% frequency (B; white arrow). Under caffeine treatment, the accumulation of YFP-RABA2A is highly irregular at the cell plate in 85% of scorable cells (C). Flufenacet treatment causes cell plate gaps, similar to those under ES7 treatment in 57% of scorable cells. In addition, aggregates of RABA2A are observed under the same treatment (D; yellow arrow). ConcA causes cell plate mislocalization and fluorescent aggregates in 88% of scorable cells (E). F to J, Dividing GFP-MAP4-labeled cells after chemical treatment. Under DMSO, the regular phragmoplast structure of GFP-MAP4 labeling is observed at a 100% frequency (F). Under ES7 treatment, the phragmoplast arrangement remains unaffected in 100% of scorable cells (G). Caffeine treatment causes abnormal phragmoplast structure in 88% of scorable cells (H). Under flufenacet treatment, GFP-MAP4 labels ectopic phragmoplast-like structures at the center of the mature cell plate in 60% of scorable cells (I). Under ConcA treatment, regular phragmoplast GFP-MAP4 labeling is observed at a 100% frequency (J). K to O, GFP-CESA3-labeled cells under chemical treatment. Under DMSO treatment, GFP-CESA3 weakly labels the mature cell plate, with high accumulation of vesicles localizing at the cell plate vicinity in 100% of scorable cells (K). ES7 treatment reduces GFP-CESA3 accumulation at the cell plate in 100% of scorable cells, and diffused fluorescent localization indicating vacuolar localization is observed (L; yellow arrow). Under caffeine treatment, GFP-CESA3 shows a strong aggregate pattern with partial localization of the aggregates at the cell plate stub in 99% of scorable cells (M; white arrow). Flufenacet treatment causes severe aggregation of GFP-CESA3 vesicles in 100% of scorable cells (N). ConcA treatment causes strong vacuolar localization of GFP-CESA3 in 100% of scorable cells (O). P to S, Immunostaining of callose after chemical treatment. Under DMSO treatment, cell plate accumulation of callose is observed at a 100% frequency (P). Under ES7 treatment, callose deposition is absent at the cell plate at a 100% frequency (Q). Similarly, caffeine treatment also reduces callose deposition in 75% of scorable cells (R). Flufenacet treatment does not affect callose deposition at the cell plate in all observed cells (S). Concentrations of chemicals are given in brackets (in μM). The respective marker fluorescence is shown in green, while FM4-64 staining of plasma membrane (A–D) and PI staining of the cell wall (F–O) are shown in magenta. Callose labeling is shown in red, while nuclei staining by DAPI is indicated in blue. Results were observed from more than 36 cells from at least four roots of each marker plant for each drug treatment. Bars = 10 μm.

of ES7 on cytokinesis restricted callose deposition and the high regulation of callose synthesis in plants.

Our biochemical analysis shows that the inhibition of callose synthase activity is consistent with a mixed-type inhibition. This effect is most likely attributable to conformational changes, which typically require high inhibitor concentrations to fully inactivate all enzyme molecules present in the mixture. The interaction of callose synthase with other regulatory proteins has been shown for the GSL6 subunit, in that it forms a complex with Rho-related protein from plants1 and DRP1 in tobacco (*Nicotiana tabacum*) Bright Yellow-2 cells (Verma and Hong, 2001). A plausible hypothesis is that ES7 binds to a specific member of the complex, but not necessarily to the catalytic subunit itself, thereby reducing the overall synthase activity at the cell plate. It is also possible that, similar to the cellulose synthase rosettes, callose synthase is a multimeric complex at the cell plate that consists of multiple GSL proteins. However, the precise composition of the callose synthase complexes and the stoichiometry of their protein components are not established in plants (Liu and Balasubramanian, 2001; Verma and Hong, 2001).

Our biochemical analysis using total Arabidopsis microsomes required a higher concentration of ES7 for substantial callose synthesis inhibition compared with Arabidopsis root meristem. The in vitro assay is performed with a detergent extract of isolated membranes from cell suspension cultures; such conditions lead to a high level of callose synthase activity in vitro upon cell disruption, much higher than that taking place in vivo, potentially due to the release of a mixture of synthases, not only those specialized in cytokinesis. In addition, it is noteworthy that the intracellular UDP-Glc concentration is estimated to be in the submillimolar (approximately 0.1–0.3 mM) or even lower range, depending on the type of cells and plant species considered (Schlupmann et al., 1994; Ito et al., 2014). Since callose synthase shows a high catalytic rate in vitro, significantly higher concentrations of substrate (at least 1 mM) than those occurring in vivo are required to perform the assay and maintain initial rate conditions in vitro. As a consequence, higher concentrations of inhibitor must be used in vitro to detect the same inhibitory effect of the drug as that observed in vivo. Overall, the data from the independent and complementary in vitro and in vivo approaches concur and both show that ES7 inhibits callose biosynthesis.

ES7 Specifically Affects Plant (1,3)-β-Glucan Biosynthesis

The specificity of ES7 for plant callose biosynthesis was verified by comparing the influence of the drug on glucan function in yeast. The yeast cell wall is primarily composed of (1,3)-β-glucans similar to plant callose together with branched (1,3;1,6)-β-glucans and mannans (Kopecká et al., 1974); however, ES7 did not provoke an inhibition of yeast cell growth. This suggests that the type of callose synthase complex active in plant cytokinesis is not shared with yeast. This is particularly remarkable, since selected plant callose synthase isoforms exhibit functional similarity with their yeast counterpart (Østergaard et al., 2002). Within the Arabidopsis callose synthase family, GSL5 partially complements the yeast callose synthase mutant (*fks1*) which mediates sensitivity to echinocandin class of antifungal glucan synthase inhibitors (Østergaard et al., 2002). GSL5 is highly accumulated in the mitogen-activated protein kinase mutant *mpk4*, which exhibits high systemic acquired resistance upon salicylic acid elicitation (Petersen et al., 2000). This emphasizes that callose accumulation in plants due to pathogen stress is more closely related to cell wall glucan formation in yeast than callose deposition during cytokinesis. Overall, our data show that ES7 does not influence cell wall formation in yeast and that different mechanisms operate in yeast and plants for glucan biosynthesis, despite the similarities of sequences between FKS1 in yeast and GSL in plants.

Time Course of Vesicular Accumulation at the CPAM

During cell plate formation, vesicles accumulate at the division plane, where they contribute to the membrane network, deliver cargo, and facilitate the removal of CPAM (Samuels et al., 1995; Jürgens, 2005; McMichael and Bednarek, 2013). However, the time-dependent contribution of cell plate-specific regulatory proteins in relation to polysaccharide deposition is poorly understood. Comparing the temporal localization of marker proteins at the CPAM with respect to callose deposition revealed a stage-dependent accumulation pattern (Fig. 9). We observed RABA2A accumulation to recede from the leading edge of the cell plate as callose deposition increased, suggesting that RABA2A vesicles contribute the major part of the membrane and cargo to the forming cell plate. These results further indicate that these vesicles are involved in neither polysaccharide deposition nor cell plate maturation. In contrast to RABA2A, KNOLLE continuously accumulated at the cell plate during callose deposition. This demonstrates that KNOLLE's function is not restricted to the fusion of the arrived post-Golgi vesicles at the early stage. KNOLLE is the main cytokinesis-specific syntaxin and is required throughout cell plate formation, including the stages of callose deposition.

Although DRP was present from early cell plate stages onward, its localization pattern did not match that of RABA2A. Strong accumulation of DRP1C was observed in the early stage but also in the late stages of cell plate maturation, concurrent with callose deposition. This corroborates previous observations of DRP presence at early stages in the absence of clathrin-coated buds and at later stages in the presence of CCVs (Gu and Verma, 1996; Otegui et al., 2001; Kang et al., 2003; Seguí-Simarro et al., 2004; Konopka et al., 2008; Ito et al., 2012; Song et al., 2012). The presense of DRP1

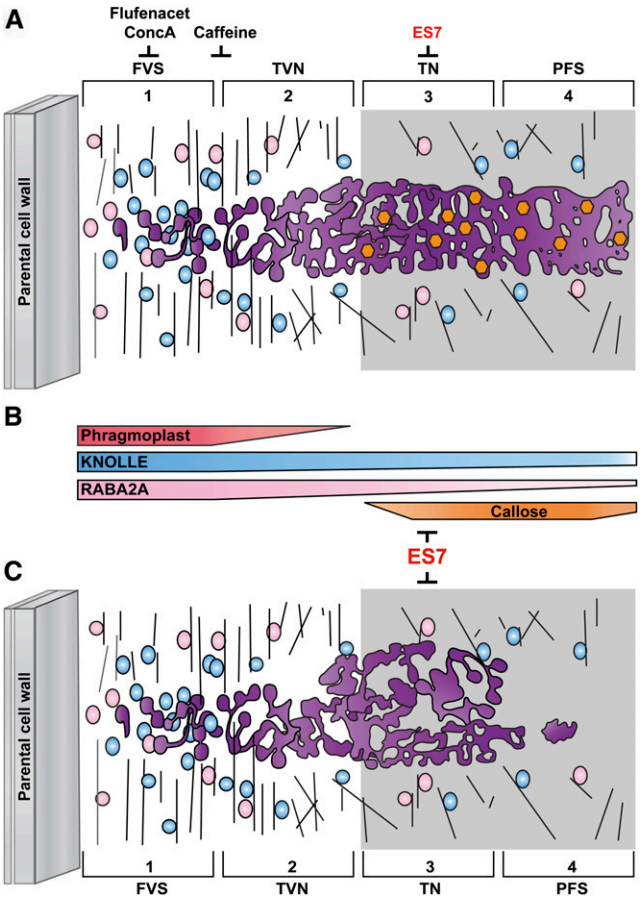

Figure 9. Proposed model of cell plate maturation and its inhibition by small molecules, including ES7. A, Cell plate formation steps and its temporal inhibition by small molecules during cell plate formation steps. In the early stage of cell plate formation (FVS), RABA2A (pink) and KNOLLE (blue) vesicles with guidance from the phragmoplast vigorously accumulate at the center of the dividing cells. While vesicles gathered at the CPAM change their structure by fusion and fission (purple tubular membrane structures in TVN), callose (orange hexagons) starts depositing at the maturing cell plate in the TN stage to support membrane structures and facilitate the transition to PFS. ES7 specifically inhibits callose synthase activity at this stage, preventing cell plate maturation. Flufenacet and ConcA affect the FVS cell plate stage, while caffeine affects the FVS-to-TVN transition stage. Corresponding references and new findings in this study are listed in Supplemental Table S1. B, Differential accumulation of cellular components during cell plate maturation. RABA2A association with the membrane is significantly reduced, while the KNOLLE levels remain constant. ES7 does have a unique mode of action, preventing further maturation steps after TVN by the inhibition of callose accumulation at the cell plate, differing markedly from that of ConcA, flufenacet, and caffeine, which have a broad range of inhibition in cellular mechanisms. C, Proposed model of an ES7-treated cell plate based on our confocal microscopy observations. Cell plate maturation after TVN is prevented by ES7 due to the inhibition of callose deposition. KNOLLE often accumulated in ectopic aggregates upon ES7 treatment, possibly due to excessive deposition of tubular membrane material.

in early cell plate stages may help concentrate the vesicle content of dumbbell-shaped vesicles, inducing the gelling of the cell plate maturing polysaccharides (Seguí-Simarro et al., 2004). However, the presence of DRP in mature stages may facilitate membrane recycling. In contrast to the case of DRP1C, the cell plate-associated accumulation of CLC2 was only observed during mature stages, concurrent with callose localization. Several recent studies established the association of DRPs with CLC, a process that is mediated by regulatory proteins at the maturing cell plate (Song et al., 2012). The presence of both proteins at this stage (i.e. during elevated callose levels) supports their role in clathrin-mediated endocytosis remodeling, including excess membrane elimination from the maturing cell plate while it is stabilized by callose.

Based on the accumulation pattern of callose and the protein markers used, we conclude that ES7 acts at the TVN/TN transition stage. Earlier stages in which callose does not accumulate were not affected by ES7. This selective behavior illustrates the temporal specificity of ES7 and indicates its activity on a highly regulatory mechanism of callose deposition and the essential role of the polysaccharide at this particular stage of cell plate development. Moreover, ES7 treatment resulted in distinct mislocalization patterns of the subcellular markers tested. KNOLLE, following chemical treatment, displayed large dilated cell plate stubs. It is plausible that, with the elimination of callose deposition, the lateral pressure and, with it, the forces that are normally exerted to ensure spatial distribution that results in an elongated shape of the TN, are missing. The presence of the KNOLLE aggregates at the periphery of the cell plate disc further supports the notion that the cell plate matures from the center outward (Samuels et al., 1995). This behavior strongly contrasts with that of CLC2, which hardly localizes at the cell plate upon ES7 treatment. This suggests that, with the arrest of cell plate maturation, the cell plate does not proceed to the stage in which CCVs are required for membrane recycling, resulting in their limited presence under chemical treatment.

ES7 Is Highly Specific in Contrast to Other Cytokinesis Inhibitors

A number of pharmacological inhibitors have been employed to disrupt cytokinesis. Direct and systematic comparison of a wide range of marker proteins provides an overview of their respective specificities (Fig. 9; Supplemental Table S1). Caffeine is one of the widely used inhibitors that disrupts cell plate formation and inhibits callose deposition at the TVN, although the exact mode of action remains unknown. One plausible mechanism is the reduction of cellular Ca^{2+} levels, given that Ca^{2+} gradients in the vicinity of the cell plate play a vital role in cytokinesis (Paul and Goff, 1973; Chen and Wolniak, 1987; Saunders and Jones, 1988; Jürgens et al., 1994). We employed relatively low concentrations of caffeine (1 mM), which affected several processes and structures (i.e. the cytoskeleton, the localization of CESA, and levels of

callose deposition). Given previous observations in which caffeine substantially reduced Ca^{2+} levels in tobacco Bright Yellow-2 cells, we inferred that Ca^{2+} levels in Arabidopsis root tips are similarly reduced (Samuels and Staehelin, 1996). An observed side effect of caffeine treatment is the inhibition of microtubule depolymerization (Yasuhara, 2005). With Ca^{2+} being important for microtubule structural integrity and activity, our observations, together with previous reports on phragmoplast depolymerization, are not altogether surprising. Furthermore, isolated phragmoplasts treated with caffeine still maintain callose biosynthetic activity (Yasuhara, 2005), raising questions about a direct inhibitory effect of caffeine on callose biosynthesis at the cell plate. Altogether, the broad effects of caffeine are a severe challenge in assessing its specific influence on callose synthesis.

The herbicide flufenacet inhibits the activity of a broad spectrum of very-long-chain fatty acid elongases, which in turn leads to organ fusion phenotypes (Trenkamp et al., 2004). Treatment of Arabidopsis seedlings with flufenacet causes cytokinetic defects observable by RABA2A mislocalization (Bach et al., 2011). The prevacuolar compartment, late endosome, and TGN are reportedly not globally affected by flufenacet (Bach et al., 2011). However, using additional markers, our data show that flufenacet caused ectopic phragmoplast accumulation at the mature cell plate and the aggregation of CESA in interphase cells. It is possible that the modification of very-long-chain fatty acids induced membrane recycling defects (Bach et al., 2011; Markham et al., 2011) and the aggregation of CESA vesicle populations. It is worth noting that callose deposition remains unaffected by flufenacet.

Treatment with ConcA results in subcellular phenotypes exhibiting changes in the Golgi morphology that include bending of cisternae, fragmentation of Golgi stacks, and aggregations of swollen vesicles in a variety of systems (Robinson et al., 2004; Dettmer et al., 2005, 2006). Thus, the cytokinesis defects are attributed to a secondary effect of total TGN-mediated trafficking interference rather than to a specific inhibition of cell plate-mediated vesicle trafficking. In our study, exposure to ConcA resulted in cytokinetic defects, observable via cell wall stubs (Reichardt et al., 2007), and caused vacuolar-type localization of CESA. ConcA is known to inhibit vacuolar acidification and to stop the degradation of GFP in the vacuole (Tamura et al., 2003). It is possible that the recycling of CESA complexes not delivered to the cell plate or the plasma membrane is blocked under ConcA exposure. As a consequence, the complexes appear to be trafficked to the vacuole, where they accumulate. In contrast to the molecules discussed above, ES7 did not affect the cytoskeleton in interphase cells or during cell division but showed specificity for callose inhibition during cell plate maturation. In ES7-treated cells undergoing division, a limited vacuolar type of CESA localization was observed. This might be a consequence of the inability of the CESA proteins to reach their target sites in the corrupted cell plate. It is apparent from our study and data in the literature that lipid composition, TGN-mediated trafficking, and callose deposition are all contributing factors to cell plate formation. We have shown that ES7 affords a direct inhibition of cytokinesis, with temporal and spatial control during cell plate maturation in plants, which cannot be achieved with previously employed inhibitors, including caffeine, flufenacet, and ConcA.

CONCLUSION

Cell plate maturation is a multifaceted process involving highly regulated membrane and cargo transport mechanisms, whose complete understanding remains challenging. By specifically inhibiting callose biosynthesis during cytokinesis with ES7, the dissection of callose deposition during cell plate maturation is possible. Given the tremendous role that cellulose synthase inhibitors such as isoxaben had in the identification of cellulose synthase subunits and contributed to our current understanding of cellulose biosynthesis (Scheible et al., 2001; Desprez et al., 2002), we expect that the unique properties of ES7 will analogously open up many avenues to dissect further callose biosynthesis during cell plate formation.

The precise molecular mechanisms by which callose synthase and callose itself are transported during cell plate formation are not understood (Chen and Kim, 2009). To date, there are no reports of live imaging of callose synthase during cytokinesis. Such experiments performed in the presence and absence of ES7 could help reveal the intermediate step of GSL trafficking to the cell plate, which might be targeted by ES7. Ongoing work toward the identification of novel trafficking-regulating components is centered on the isolation and characterization of the vesicular cargo (Drakakaki et al., 2012) at the individual stages of cytokinesis. Overall, we expect that the inhibitory qualities of ES7 will guide future research into the role of callose synthase in plant cytokinesis, leading to a comprehensive understanding of this vital process for plant growth and development.

MATERIALS AND METHODS

Plant Materials and Growth

All Arabidopsis (*Arabidopsis thaliana*) seedlings were grown as described previously (Park and Nebenführ, 2013). Briefly, seeds were germinated on square plates containing Murashige and Skoog (MS) medium (Sigma; one-quarter strength) supplemented with 1% (w/v) Suc, pH adjusted to 5.7, and solidified with 0.5% (w/v) phytagel (Sigma) and designated chemicals. Plates were incubated at 10° off vertical in a growth room with a 16-h-light/8-h-dark photoperiod for 3 to 5 d as specified in the next paragraph. Transgenic lines expressing YFP-RABA2A (Chow et al., 2008), KNOLLE-GFP (Reichardt et al., 2007), DRP1C-GFP (Konopka et al., 2008), CLC2-GFP (Konopka et al., 2008), GFP-MAP4 (Marc et al., 1998), GFP-CESA3 (Desprez et al., 2007), and Brassinosteroid-Insensitive1-GFP (Geldner et al., 2007) were used to observe subcellular phenotypes upon chemical treatment.

Chemical Treatment

For microscopy, seedlings were grown as described above for 3 d and then transferred to 48-well plates containing 2 mL of liquid MS medium supplemented with 390 mM DMSO (Sigma), 1 μM ConcA (Sigma), 100 nM flufenacet (Sigma), 50 μM (or desired concentration) ES7 (Chembridge), or 1 mM caffeine (Sigma). Chemicals were diluted to their working concentrations from either 1,000× stock solutions for flufenacet (DMSO) and ES7 (DMSO) or 100× stock solutions for ConcA (DMSO) and caffeine (water). Pulse treatments of Arabidopsis seedlings were performed for 2 h in the presence of the desired chemicals. Seedlings were either immediately observed with the microscope or fixed with 4% (w/v) paraformaldehyde (Electron Microscopy Sciences) in a microtubule-stabilizing buffer composed of 50 mM PIPES, 2 mM EGTA, and 2 mM $MgSO_4$. Fixation was performed in a two-step process involving an initial treatment under vacuum for 15 min followed by an overnight incubation at 4°C at atmospheric pressure.

Root Growth Measurements

For root growth assays, seedlings were grown on vertical plates as described above. Plates were scanned using a flatbed scanner (Epson Perfection V300) at days 3, 4, and 5 after germination, and root lengths were measured using the segmented line tool in the image-analysis software package ImageJ (National Institutes of Health). Statistical analyses and graphic visualization were carried out in Prism 6.0 (GraphPad).

Immunostaining of Callose

Three-day-old seedlings expressing the different fluorescent markers listed above were treated with the pharmacological compounds and fixed in 4% (v/v) paraformaldehyde. Samples were washed once with microtubule-stabilizing buffer and transferred into medium baskets of an InsituPro VSi instrument (Intavis) for automated in situ hybridization and immunohistochemistry or stored at 4°C for later use. A standard protocol for basic whole-mounted Arabidopsis seedlings was used (Sauer and Friml, 2010). Briefly, samples were successively washed three times with phosphate-buffered saline containing 0.1% (v/v) Triton X-100, incubated in 2% (w/v) Driselase (Sigma) for 45 min at 37°C for cell wall hydrolysis, and treated with 10% (v/v) DMSO and 3% (v/v) octylphenoxypolyethoxyethanol (IGEPAL CA-630; Sigma) in phosphate-buffered saline containing 0.1% (v/v) Triton X-100 for membrane permeabilization. Mouse monoclonal antibody against callose (BioSupplies) was used at a dilution of 1:2,000, while the secondary antibody, a goat anti-mouse IgG conjugated to Cy3 (Invitrogen), was used at a 1:500 dilution. Samples were mounted in Citifluor AF1 antifadent mountant medium (Electron Microscopy Sciences) in the presence of 1 $\mu g\ mL^{-1}$ 4′,6-diamidino-2-phenylindole (DAPI) and imaged immediately.

Confocal Laser Scanning Microscopy

Three confocal laser scanning microscopes were used throughout this study. A TCS SP2 (Leica Microsystems) and a LSM710 (Carl Zeiss) were used for live-cell imaging following chemical treatment and immunolabeling of Arabidopsis roots. At least 15 roots for each marker plant were imaged from more than two experimental repeats. FM4-64 (Invitrogen) was used as a counterstain of plasma membrane in live cells. A 488-nm argon laser was used to excite GFP and FM4-64. A 561-nm diode laser was used for Cy3 and propidium iodide (PI; Sigma), and a 405-nm diode laser was used for DAPI and Aniline Blue (Sigma). Emissions were collected over a wavelength range of 492 to 545 nm for GFP, 620 to 700 nm for FM4-64, 550 to 600 nm for Cy3, 430 to 480 nm for DAPI, 450 to 510 nm for Aniline Blue, and 650 to 750 nm for PI. For multicolor imaging, the sequential line-scanning mode was employed with either a 40× 1.1 numerical aperture (NA) water-immersion objective or a 63× 1.4 NA oil-immersion objective. An LSM700 (Carl Zeiss) was used for imaging whole root and leaf cell morphology (20× 0.8 NA objective) with FM4-64 and PI staining, respectively. For immunostaining of callose at the root cells, after the immunostaining described above, Z-series of the whole root tip in optical sections of 0.5-μm intervals were imaged using an LSM710 equipped with a 40× 1.1 NA water-immersion objective. The Zen 2012 software (Carl Zeiss) was used for three-dimensional rendering.

Detergent Extraction of Membrane Proteins and Callose Synthase Assay

Arabidopsis cell suspension cultures from the Flanders Institute for Biotechnology Plant Systems Biology Department (Landsberg *erecta*, PSB-D line) at the University of Ghent were a generous gift of Dr. Jiří Friml. The cell suspension cultures were grown in MS medium containing minimal organics (Sigma) supplemented with 3% (w/v) Suc, 0.05 mg L^{-1} naphthaleneacetic acid, and 0.005 mg L^{-1} kinetin. Cells were harvested after 7 d of culture in the dark at 25°C under constant agitation on a rotary shaker (120 oscillations min^{-1}). CHAPS extracts of microsomal membranes were prepared using a final detergent concentration of 1% (v/v) as described previously (Him et al., 2001). Callose synthase activity was assayed using the supernatant recovered after centrifugation at 150,000*g* for 1 h. Activity was measured in a total volume of 200 μL in the presence of 0 to 100 μM ES7. Typical reaction mixtures consisted of 100 μL of CHAPS extract, 352 mM DMSO (solvent of ES7), 100 mM MOPS/NaOH buffer (pH 6.8), 8 mM $CaCl_2$, and a mixture of UDP-Glc and UDP-[U-^{14}C]Glc (250 mCi $mmol^{-1}$; Perkin-Elmer) to reach the final concentrations of substrate specified in earlier protocols (Fig. 1 in Him et al., 2001). The assays were performed in triplicate at 22°C, and the experiments were repeated twice. The reactions were stopped by adding 400 μL of absolute ethanol either after 1 h or, in the case of enzyme kinetic assays, after 5, 10, 20, and 40 min. The polysaccharide synthesized in vitro was precipitated at −20°C for 16 h. The radioactive ethanol-insoluble polysaccharide was recovered by filtration on glass-fiber filters (Millipore) and subsequently washed with 4 mL of water and 4 mL of absolute ethanol. Using a liquid scintillation counter, the radioactivity retained in the filters was measured in 4 mL of the liquid scintillation cocktail. The enzyme kinetics were fitted according to the Michaelis-Menten model.

Supplemental Data

The following materials are available in the online version of this article.

Supplemental Figure S1. Schematic illustration of cell plate formation.

Supplemental Figure S2. 3D rendering of YFP-RABA2A cell plate localization upon ES7 treatment.

Supplemental Figure S3. Effect of ES7 on callose deposition in various plant tissues.

Supplemental Figure S4. ES7 is a plant-specific cytokinesis inhibitor.

Supplemental Figure S5. Cellulose localization remains unaffected under ES7 treatment.

Supplemental Figure S6. Effects of selected cytokinesis inhibitors on the localization of GFP-CESA3 and GFP-MAP4 in interphase cells.

Supplemental Table S1. Summary of markers and inhibitors used in this study.

Supplemental Movie S1. 3D rendering of YFP-RABA2A cell plate localization in DMSO.

Supplemental Movie S2. 3D rendering of KNOLLE-GFP cell plate localization in DMSO.

Supplemental Movie S3. 3D rendering of YFP-RABA2A cell plate localization upon ES7 treatment.

Supplemental Movie S4. 3D rendering of KNOLLE-GFP cell plate localization upon ES7 treatment.

ACKNOWLEDGMENTS

We thank Drs. Ian Moore (University of Oxford), Gerd Jürgens (Max Planck Institute for Developmental Biology), Sebastian Bednarek (University of Wisconsin), Danniel Van Damme (Flanders Institute for Biotechnology), Samantha Vernhettes (Institut National de la Recherche Agronomique), Joshua Heazlewood (Joint Bioenergy Institute) and Arabidopsis Biological Resource Center for sharing seed stocks of fluorescent markers, antibodies and mutants. We also thank Dr. Jiří Friml (Flanders Institute for Biotechnology and Institute of Science and Technology Austria) for providing the Arabidopsis cell suspension cultures; Dr. William Lucas (University of California, Davis) for sharing the Leica SP2 microscope; Drs. Marcela Rojas-Pierce (North Carolina State

University), Bo Liu (University of California, Davis) and Natasha Raikhel (University of California, Riverside) for critically reading this article; and members of the Drakakaki laboratory for helpful discussions.

Received April 18, 2014; accepted May 19, 2014; published May 23, 2014.

LITERATURE CITED

Albersheim P, Darvill A, Roberts K, Sederoff R, Staehelin LA (2010) Plant Cell Walls. Garland Science, New York

Assaad FF, Huet Y, Mayer U, Jürgens G (2001) The cytokinesis gene KEULE encodes a Sec1 protein that binds the syntaxin KNOLLE. J Cell Biol **152:** 531–543

Bach L, Gissot L, Marion J, Tellier F, Moreau P, Satiat-Jeunemaître B, Palauqui JC, Napier JA, Faure JD (2011) Very-long-chain fatty acids are required for cell plate formation during cytokinesis in Arabidopsis thaliana. J Cell Sci **124:** 3223–3234

Bassham DC, Blatt MR (2008) SNAREs: cogs and coordinators in signaling and development. Plant Physiol **147:** 1504–1515

Chen TL, Wolniak SM (1987) Lithium induces cell plate dispersion during cytokinesis in Tradescantia. Protoplasma **141:** 56–63

Chen XY, Kim JY (2009) Callose synthesis in higher plants. Plant Signal Behav **4:** 489–492

Chen XY, Liu L, Lee E, Han X, Rim Y, Chu H, Kim SW, Sack F, Kim JY (2009) The Arabidopsis callose synthase gene *GSL8* is required for cytokinesis and cell patterning. Plant Physiol **150:** 105–113

Chow CM, Neto H, Foucart C, Moore I (2008) Rab-A2 and Rab-A3 GTPases define a *trans*-Golgi endosomal membrane domain in *Arabidopsis* that contributes substantially to the cell plate. Plant Cell **20:** 101–123

Collings DA, Gebbie LK, Howles PA, Hurley UA, Birch RJ, Cork AH, Hocart CH, Arioli T, Williamson RE (2008) Arabidopsis dynamin-like protein DRP1A: a null mutant with widespread defects in endocytosis, cellulose synthesis, cytokinesis, and cell expansion. J Exp Bot **59:** 361–376

Desprez T, Juraniec M, Crowell EF, Jouy H, Pochylova Z, Parcy F, Höfte H, Gonneau M, Vernhettes S (2007) Organization of cellulose synthase complexes involved in primary cell wall synthesis in Arabidopsis thaliana. Proc Natl Acad Sci USA **104:** 15572–15577

Desprez T, Vernhettes S, Fagard M, Refrégier G, Desnos T, Aletti E, Py N, Pelletier S, Höfte H (2002) Resistance against herbicide isoxaben and cellulose deficiency caused by distinct mutations in same cellulose synthase isoform CESA6. Plant Physiol **128:** 482–490

Dettmer J, Hong-Hermesdorf A, Stierhof YD, Schumacher K (2006) Vacuolar H^+-ATPase activity is required for endocytic and secretory trafficking in *Arabidopsis*. Plant Cell **18:** 715–730

Dettmer J, Schubert D, Calvo-Weimar O, Stierhof YD, Schmidt R, Schumacher K (2005) Essential role of the V-ATPase in male gametophyte development. Plant J **41:** 117–124

Dhonukshe P, Baluska F, Schlicht M, Hlavacka A, Samaj J, Friml J, Gadella TW Jr (2006) Endocytosis of cell surface material mediates cell plate formation during plant cytokinesis. Dev Cell **10:** 137–150

Drakakaki G, Robert S, Szatmari AM, Brown MQ, Nagawa S, Van Damme D, Leonard M, Yang Z, Girke T, Schmid SL, et al (2011) Clusters of bioactive compounds target dynamic endomembrane networks in vivo. Proc Natl Acad Sci USA **108:** 17850–17855

Drakakaki G, van de Ven W, Pan S, Miao Y, Wang J, Keinath NF, Weatherly B, Jiang L, Schumacher K, Hicks G, et al (2012) Isolation and proteomic analysis of the SYP61 compartment reveal its role in exocytic trafficking in Arabidopsis. Cell Res **22:** 413–424

Dröse S, Bindseil KU, Bowman EJ, Siebers A, Zeeck A, Altendorf K (1993) Inhibitory effect of modified bafilomycins and concanamycins on P- and V-type adenosinetriphosphatases. Biochemistry **32:** 3902–3906

El Kasmi F, Krause C, Hiller U, Stierhof YD, Mayer U, Conner L, Kong L, Reichardt I, Sanderfoot AA, Jürgens G (2013) SNARE complexes of different composition jointly mediate membrane fusion in Arabidopsis cytokinesis. Mol Biol Cell **24:** 1593–1601

Fagard M, Desnos T, Desprez T, Goubet F, Refregier G, Mouille G, McCann M, Rayon C, Vernhettes S, Höfte H (2000) *PROCUSTE1* encodes a cellulose synthase required for normal cell elongation specifically in roots and dark-grown hypocotyls of *Arabidopsis*. Plant Cell **12:** 2409–2424

Fujimoto M, Arimura S, Ueda T, Takanashi H, Hayashi Y, Nakano A, Tsutsumi N (2010) Arabidopsis dynamin-related proteins DRP2B and DRP1A participate together in clathrin-coated vesicle formation during endocytosis. Proc Natl Acad Sci USA **107:** 6094–6099

Geldner N, Hyman DL, Wang X, Schumacher K, Chory J (2007) Endosomal signaling of plant steroid receptor kinase BRI1. Genes Dev **21:** 1598–1602

Gu X, Verma DP (1996) Phragmoplastin, a dynamin-like protein associated with cell plate formation in plants. EMBO J **15:** 695–704

Guseman JM, Lee JS, Bogenschutz NL, Peterson KM, Virata RE, Xie B, Kanaoka MM, Hong Z, Torii KU (2010) Dysregulation of cell-to-cell connectivity and stomatal patterning by loss-of-function mutation in Arabidopsis chorus (glucan synthase-like 8). Development **137:** 1731–1741

Heese M, Gansel X, Sticher L, Wick P, Grebe M, Granier F, Jurgens G (2001) Functional characterization of the KNOLLE-interacting t-SNARE AtSNAP33 and its role in plant cytokinesis. J Cell Biol **155:** 239–249

Him JL, Pelosi L, Chanzy H, Putaux JL, Bulone V (2001) Biosynthesis of (1→3)-beta-D-glucan (callose) by detergent extracts of a microsomal fraction from Arabidopsis thaliana. Eur J Biochem **268:** 4628–4638

Hong Z, Delauney AJ, Verma DP (2001) A cell plate-specific callose synthase and its interaction with phragmoplastin. Plant Cell **13:** 755–768

Huss M, Ingenhorst G, König S, Gassel M, Dröse S, Zeeck A, Altendorf K, Wieczorek H (2002) Concanamycin A, the specific inhibitor of V-ATPases, binds to the V(o) subunit c. J Biol Chem **277:** 40544–40548

Ito E, Fujimoto M, Ebine K, Uemura T, Ueda T, Nakano A (2012) Dynamic behavior of clathrin in Arabidopsis thaliana unveiled by live imaging. Plant J **69:** 204–216

Ito J, Herter T, Baidoo EE, Lao J, Vega-Sánchez ME, Smith-Moritz AM, Adams PD, Keasling JD, Usadel B, Petzold CJ, et al (2014) Analysis of plant nucleotide sugars by hydrophilic interaction liquid chromatography and tandem mass spectrometry. Anal Biochem **448:** 14–22

Jones MG, Payne HL (1978) Cytokinesis in Impatiens balsamina and the effect of caffeine. Cytobios **20:** 79–91

Jürgens G (2005) Cytokinesis in higher plants. Annu Rev Plant Biol **56:** 281–299

Jürgens M, Hepler LH, Rivers BA, Hepler PK (1994) BAPTA-calcium buffers modulate cell plate formation in stamen hairs of *Tradescantia*: evidence for calcium gradients. Protoplasma **183:** 86–99

Kang BH, Busse JS, Bednarek SY (2003) Members of the *Arabidopsis* dynamin-like gene family, ADL1, are essential for plant cytokinesis and polarized cell growth. Plant Cell **15:** 899–913

Konopka CA, Backues SK, Bednarek SY (2008) Dynamics of *Arabidopsis* dynamin-related protein 1C and a clathrin light chain at the plasma membrane. Plant Cell **20:** 1363–1380

Konopka CA, Bednarek SY (2008) Comparison of the dynamics and functional redundancy of the Arabidopsis dynamin-related isoforms DRP1A and DRP1C during plant development. Plant Physiol **147:** 1590–1602

Kopecká M, Phaff HJ, Fleet GH (1974) Demonstration of a fibrillar component in the cell wall of the yeast Saccharomyces cerevisiae and its chemical nature. J Cell Biol **62:** 66–76

Lauber MH, Waizenegger I, Steinmann T, Schwarz H, Mayer U, Hwang I, Lukowitz W, Jürgens G (1997) The Arabidopsis KNOLLE protein is a cytokinesis-specific syntaxin. J Cell Biol **139:** 1485–1493

Liu J, Balasubramanian MK (2001) 1,3-β-Glucan synthase: a useful target for antifungal drugs. Curr Drug Targets Infect Disord **1:** 159–169

Marc J, Granger CL, Brincat J, Fisher DD, Kao Th, McCubbin AG, Cyr RJ (1998) A *GFP-MAP4* reporter gene for visualizing cortical microtubule rearrangements in living epidermal cells. Plant Cell **10:** 1927–1940

Markham JE, Molino D, Gissot L, Bellec Y, Hématy K, Marion J, Belcram K, Palauqui JC, Satiat-Jeunemaître B, Faure JD (2011) Sphingolipids containing very-long-chain fatty acids define a secretory pathway for specific polar plasma membrane protein targeting in *Arabidopsis*. Plant Cell **23:** 2362–2378

McMichael CM, Bednarek SY (2013) Cytoskeletal and membrane dynamics during higher plant cytokinesis. New Phytol **197:** 1039–1057

Miart F, Desprez T, Biot E, Morin H, Belcram K, Hofte H, Gonneau M, Vernhettes S (2014) Spatio-temporal analysis of cellulose synthesis during cell plate formation in Arabidopsis. Plant J**77:** 71–84

Østergaard L, Petersen M, Mattsson O, Mundy J (2002) An Arabidopsis callose synthase. Plant Mol Biol **49:** 559–566

Otegui MS, Mastronarde DN, Kang BH, Bednarek SY, Staehelin LA (2001) Three-dimensional analysis of syncytial-type cell plates during endosperm cellularization visualized by high resolution electron tomography. Plant Cell **13:** 2033–2051

Otegui MS, Staehelin LA (2004) Electron tomographic analysis of postmeiotic cytokinesis during pollen development in Arabidopsis thaliana. Planta **218:** 501–515

Park E, Nebenführ A (2013) Myosin XIK of Arabidopsis thaliana accumulates at the root hair tip and is required for fast root hair growth. PLoS ONE **8:** e76745

Paul DC, Goff CW (1973) Comparative effects of caffeine, its analogues and calcium deficiency on cytokinesis. Exp Cell Res **78:** 399–413

Petersen M, Brodersen P, Naested H, Andreasson E, Lindhart U, Johansen B, Nielsen HB, Lacy M, Austin MJ, Parker JE, et al (2000) Arabidopsis MAP kinase 4 negatively regulates systemic acquired resistance. Cell **103:** 1111–1120

Reichardt I, Stierhof YD, Mayer U, Richter S, Schwarz H, Schumacher K, Jürgens G (2007) Plant cytokinesis requires de novo secretory trafficking but not endocytosis. Curr Biol **17:** 2047–2053

Robinson DG, Albrecht S, Moriysu Y (2004) The V-ATPase inhibitors concanamycin A and bafilomycin A lead to Golgi swelling in tobacco BY-2 cells. Protoplasma **224:** 255–260

Samuels AL, Giddings TH Jr, Staehelin LA (1995) Cytokinesis in tobacco BY-2 and root tip cells: a new model of cell plate formation in higher plants. J Cell Biol **130:** 1345–1357

Samuels AL, Staehelin LA (1996) Caffeine inhibits cell plate formation by disrupting membrane reorganization just after the vesicle fusion step. Protoplasma **195:** 144–155

Sauer M, Friml JÌ (2010) Immunolocalization of proteins in plants. Methods Mol Biol **655:** 253–263

Saunders MJ, Jones KJ (1988) Distortion of plant cell plate formation by the intracellular-calcium antagonist TMB-8. Protoplasma **144:** 92–100

Scheible WR, Eshed R, Richmond T, Delmer D, Somerville C (2001) Modifications of cellulose synthase confer resistance to isoxaben and thiazolidinone herbicides in Arabidopsis Ixr1 mutants. Proc Natl Acad Sci USA **98:** 10079–10084

Schlupmann H, Bacic A, Read SM (1994) Uridine diphosphate glucose metabolism and callose synthesis in cultured pollen tubes of *Nicotiana alata* Link et Otto. Plant Physiol **105:** 659–670

Seguí-Simarro JM, Austin JR II, White EA, Staehelin LA (2004) Electron tomographic analysis of somatic cell plate formation in meristematic cells of *Arabidopsis* preserved by high-pressure freezing. Plant Cell **16:** 836–856

Söllner R, Glässer G, Wanner G, Somerville CR, Jürgens G, Assaad FF (2002) Cytokinesis-defective mutants of Arabidopsis. Plant Physiol **129:** 678–690

Song K, Jang M, Kim SY, Lee G, Lee GJ, Kim DH, Lee Y, Cho W, Hwang I (2012) An A/ENTH domain-containing protein functions as an adaptor for clathrin-coated vesicles on the growing cell plate in Arabidopsis root cells. Plant Physiol **159:** 1013–1025

Staehelin LA, Hepler PK (1996) Cytokinesis in higher plants. Cell **84:** 821–824

Tamura K, Shimada T, Ono E, Tanaka Y, Nagatani A, Higashi SI, Watanabe M, Nishimura M, Hara-Nishimura I (2003) Why green fluorescent fusion proteins have not been observed in the vacuoles of higher plants. Plant J **35:** 545–555

Thiele K, Wanner G, Kindzierski V, Jürgens G, Mayer U, Pachl F, Assaad FF (2009) The timely deposition of callose is essential for cytokinesis in Arabidopsis. Plant J **58:** 13–26

Trenkamp S, Martin W, Tietjen K (2004) Specific and differential inhibition of very-long-chain fatty acid elongases from Arabidopsis thaliana by different herbicides. Proc Natl Acad Sci USA **101:** 11903–11908

Van Damme D, Gadeyne A, Vanstraelen M, Inzé D, Van Montagu MC, De Jaeger G, Russinova E, Geelen D (2011) Adaptin-like protein TPLATE and clathrin recruitment during plant somatic cytokinesis occurs via two distinct pathways. Proc Natl Acad Sci USA **108:** 615–620

Verma DP, Hong Z (2001) Plant callose synthase complexes. Plant Mol Biol **47:** 693–701

Worden N, Park E, Drakakaki G (2012) Trans-Golgi network: an intersection of trafficking cell wall components. J Integr Plant Biol **54:** 875–886

Yasuhara H (2005) Caffeine inhibits callose deposition in the cell plate and the depolymerization of microtubules in the central region of the phragmoplast. Plant Cell Physiol **46:** 1083–1092

Zhang L, Zhang H, Liu P, Hao H, Jin JB, Lin J (2011) Arabidopsis R-SNARE proteins VAMP721 and VAMP722 are required for cell plate formation. PLoS ONE **6:** e26129

Zheng H, Bednarek SY, Sanderfoot AA, Alonso J, Ecker JR, Raikhel NV (2002) NPSN11 is a cell plate-associated SNARE protein that interacts with the syntaxin KNOLLE. Plant Physiol **129:** 530–539